Triple-Color Coincidence Analysis: One Step Further in Following Higher Order Molecular Complex Formation

Katrin G. Heinze,* Michael Jahnz,† and Petra Schwille†
*Biophysics Institute/BioTec, Dresden University of Technology, Dresden, Germany; and †Experimental Biophysics Group, Max-Planck-Institute for Biophysical Chemistry, Göttingen, Germany

ABSTRACT Confocal fluorescence spectroscopy is a versatile method for studying dynamics and interactions of biomolecules in their native environment with minimal interference with the observed system. Analyzing coincident fluctuations induced by single molecule movement in spectrally distinct detection channels, dual-color fluorescence cross-correlation, and coincidence analysis have proven most powerful for probing the formation or cleavage of molecular bonds in real time. The similarity of the optical setup with those used for laser scanning microscopy, as well as the non-invasiveness of the methods, make them easily adaptive for intracellular measurements, to observe the association and dissociation of biomolecules in situ. However, in contrast to standard fluorescence microscopy, where multiple fluorophores can be spectrally resolved, single molecule detection has so far been limited to dual-color detection systems due to the harsh requirements on detection sensitivity. In this study, we show that under certain experimental conditions, employing simultaneous two-photon excitation of three distinct dye species, their successful discrimination indeed becomes possible even on a single molecule level. This enables the direct observation of higher order molecular complex formation in the confocal volume. The theoretical concept of triple-color coincidence analysis is outlined in detail, along with an experimental demonstration of its principles utilizing a simple nucleic acid reaction system.

INTRODUCTION

Fluorescence microscopy and spectroscopy have in recent years made a tremendous impact in the study of molecular localization, trafficking, and interactions in live cells and can thus be considered major biophysical tools for the elucidation of protein function and dynamics. Particularly powerful are the many application modes of confocal or two-photon laser scanning microscopy that allow us to map out a whole cell for multiple fluorescent species with extremely high precision and submicrometer resolution, but also large specificity of detection (Pawley, 1995). The availability of high-end confocal microscopes and specifically developed fluorophores meanwhile routinely supports the simultaneous imaging of three or even more different molecular species in a single cell, their precise quantitation and localization being a crucial requirement for all studies on protein communication and networking, supposedly the main pillars of cellular metabolism and signaling. However, one of the most crucial tasks for elucidating the functional dynamics of proteins in their cellular environment, i.e., the direct detection of protein-protein interactions in situ, is still a challenging problem far from being generally solved in a satisfactory fashion (Lippincott-Schwartz et al., 2001). A first check for molecular interactions can be performed by the so-called colocalization analysis (Manders et al., 1993), which is nowadays supported by most commercial confocal microscopes. It compares images recorded in spectrally distinct detection channels, reflecting different molecular species. Although there is certainly some justification in assuming that interacting molecules globally tend to localize at common sites, colocalization can by no means be a sufficient condition to postulate true molecular interaction. In addition to that, quantitation of image superposition can be rather tedious. Image correlation analysis and other image processing algorithms (Peterson et al., 1986; Demandolx and Davoust, 1997; Wiseman et al., 2000) have thus recently been evoked, in particular to eliminate artifacts induced by spectral crosstalk, one of the major obstacles and source of false-positive results. However, none of these strategies can circumvent the intrinsic shortcoming of colocalization analysis that the mere presence of two molecules at the same spatial position does not necessarily imply mutual recognition.

This ambiguity can be avoided by employing another presently very popular and immensely powerful fluorescence-related tool to study molecular interactions: fluorescence resonance energy transfer (FRET; Clegg, 1996; Periasamy, 1998; Wouters et al., 2001; Selvin, 2002). The idea behind it is that by bringing two fluorescent probes of different spectroscopic properties in close distance, radiationless energy transfer from an energetically higher primarily excited molecule to an energetically lower one is highly probable. FRET shifts the emission of the total system to longer wavelengths and thus encodes molecular distance by the spectral properties of the emitted light. Since the molecular distances which can be resolved by FRET are for standard fluorophore combinations in the visible spectral range of the order of several 10 Å, corresponding to the average size of many proteins or protein complexes, FRET is a much more reliable tool to probe a kind of proximity that can only be gained by tight molecular interaction. Its only limitation is the rather narrow distance range in which sub-

Submitted May 22, 2003, and accepted for publication September 2, 2003.
Address reprint requests to Petra Schwille, E-mail: pschwil@mpi-cbg.de.

0006-3495/04/01/506/11 $2.00

stantial FRET efficiencies can be obtained, imposing constraints on the overall size of the molecular complex, but also on the labeling procedure: the dyes have to be attached to protein residues close enough to be affected by the binding, but far enough away from the binding site not to interfere with the recognition process.

An alternative to the previous approaches is provided by means of confocal single molecule fluctuation analysis (Eigen and Rigler, 1994), the technical basis for fluorescence correlation spectroscopy (FCS; Magde et al., 1972) or confocal coincidence analysis (Winkler et al.,1999). These techniques rely on the statistical evaluation of fluorescence signal fluctuations, induced by the passage of single freely diffusing particles through a laser-illuminated focal volume element of submicrometer dimensions. Autocorrelating one fluctuating signal, molecular concentrations, mobility coefficients, and rates of inter- and intramolecular dynamics can be precisely determined (Elson and Magde, 1974). Cross-correlating two distinct signals, e.g., emissions in two spectral ranges, underlying mechanisms that relate the two signals to each other can be resolved (Schwille et al., 1997). Dual-color cross-correlation, or the conceptually simpler coincidence analysis (Winkler et al., 1999; Heinze et al., 2002) thus provides an excellent means to follow molecular interactions between two differently labeled species, as the presence of coincident signal fluctuations in two distinct emission channels unequivocally indicate the transit of two concomitantly moving, and thus tightly linked, molecules. Dual-color cross-correlation analysis has been successfully applied to study association reactions (Schwille et al., 1997), enzymatic digestion of double-labeled substrate (Kettling et al., 1998), and molecular aggregate formation (Bieschke et al., 2000). It has also been employed to analyze PCR reactions (Rigler et al., 1998) and to study toxin endocytosis in live cells (Bacia et al., 2002). Recently, it has been demonstrated that dual-color confocal analysis can be performed with a single excitation line by employing two-photon excitation, since the broad two-photon absorption spectra of many standard dyes show a large overlap even for largely different emission properties (Heinze et al., 2000). Two photon cross-correlation and coincidence analysis (Heinze et al., 2002) provides the same features as the conventional instrumentation with two excitation lines, but with significant advantages concerning simplicity and stability of the setup. Moreover, its application to intracellular systems shows several known benefits such as increased penetration, less scattering and reduced cumulative photobleaching (Denk et al., 1990, Schwille et al., 1999).

The encouraging results obtained by two-photon excited dual-color schemes motivated a further extension of the technique to encompass additional spectral dimensions, as the problems usually arising from spectral separation of multiple excitation and emission ranges are dramatically reduced with only one excitation line in the near infrared (IR). The scope of this study is thus, to provide both the theoretical framework and the experimental realization of triple-color analysis on a single molecular level in solution, based on coincident fluctuations in three independent measurement channels induced by diffusing ternary or higher complexes. It can be shown that the calculation of the second- and third-order coincidence factors allows a quantitative evaluation of absolute concentrations of triple-labeled molecules in the presence of single- and dual-labeled ones, and thus opens up exciting perspectives for the study of more complex processes occurring in live cells.

MATERIALS AND METHODS

Theoretical concept of triple-color correlation analysis

The basic idea behind multicolor coincidence analysis is to distinguish multipally-labeled particles, emerging as the product of higher order complex formation, by the coincident signal fluctuations in spectrally distinct detection channels due to the diffusion of the complexed molecules through the common observation volume. For this principle to become effective, it is imperative that the average number of molecules simultaneously observed be of the order of one, as only under these conditions can fluctuation analysis be sensibly performed. Obviously, the probability for coincident fluctuations arising from independent molecules traversing the detection volume at exactly the same instance is basically zero, such that every true coincidence event indicates the presence of a complex particle. If the measurement time is long enough for sufficient averaging, the relative concentration of ternary- and binary-labeled complexes can be quantitatively determined from the number of triple and dual coincidences relative to the total number of molecular transits in all observation channels.

The time-dependent fluorescence signal $F_i(t)$ induced by a fluorescent species i in the respective detection channel is determined by the number of molecules simultaneously present in the measurement volume, N_i, and their molecular brightness values, η_i, as

$$F_i(t) = \eta_i N_i(t), \tag{1}$$

with N_i being the product of the local concentration C_i and the effective volume element V_{eff}, such that

$$N_i(t) = C_i(t) V_{eff}. \tag{2}$$

For two-photon excitation, the effective volume size is $V_{eff} = (\pi/2)^{3/2} r_0^2 z_0$ with r_0 and z_0 as the $1/e^2$ values of the illumination intensity distribution $I_{ex}(r)$, which is assumed to be Gaussian in all three dimensions.

If the system consists of three different molecular species in the blue, green, and red with numbers N_b, N_g, and N_r, as well as their dual and triple combinations, N_{bg}, N_{gr}, N_{rb}, and N_{bgr}, the representative fluorescence signal recorded by, e.g., the blue detection channel b (with respective results for g and r), is now given by

$$F_b(t) = \eta_b(N_b(t) + N_{bg}(t) + N_{rb}(t) + N_{bgr}(t)) \equiv \eta_b N_{b,tot}(t). \tag{3}$$

For every combination of two detection channels, the dual cross-correlation functions can be calculated as (i and j being permutations of b, g, and r)

$$G_{ij}(\tau) = \langle \delta F_i(t) \delta F_j(t+\tau) \rangle / (\langle F_i \rangle \langle F_j \rangle), \tag{4}$$

with the respective autocorrelation functions recorded from the single channels being the normalized variances of the measurement signals,

$$G_i(\tau) = \langle \delta F_i(t)\delta F_i(t+\tau)\rangle / \langle F_i\rangle^2, \quad (5)$$

$$G_i(0) = \left\langle \delta N_{i,tot}^2(t)\right\rangle \Big/ N_{i,tot}^2. \quad (6)$$

In the low concentration regime, the probability for detecting N_i molecules of species i (b, g, r, bg, gr, rb, and bgr) in the volume element V_{eff} at any time is governed by Poissonian statistics, as

$$P(x_i = N_i(t)) = \frac{N_i^{x_i}\exp^{-N_i}}{x_i!}. \quad (7)$$

The Poisson distribution of a certain parameter has the unique property that its variance equals the mean. Thus, the insertion of Eq. 3 in Eq. 4 yields a rather simple expression. The variances for species i are given by

$$Var(P(x_i)) = \sigma_i^2 = \left\langle \delta N_i^2(t)\right\rangle = \langle N_i\rangle, \quad (8)$$

whereas the mixed terms ($i \neq j$) cancel out as

$$\langle \delta N_i(0)\delta N_j(0)\rangle = 0. \quad (9)$$

In dual-color experiments, the average number of double-labeled particles in the measurement volume can thus be determined from the amplitudes of auto- and cross-correlation amplitudes according to the simple relationship (Schwille, 2001) of

$$\langle N_{ij}\rangle = G_{ij}(0)/(G_i(0)G_j(0)). \quad (10)$$

With $N_{i,tot}$ as defined in Eq. 3, autocorrelation amplitudes in ternary mixtures as outlined above are given by

$$G_i(0) = 1/\langle N_{i,tot}\rangle, \quad (11)$$

($i = b$, g, and r), whereas the following dual cross-correlation amplitudes are obtained as

$$G_{bg}(0) = (\langle N_{bg}\rangle + \langle N_{bgr}\rangle)/(\langle N_{b,tot}\rangle\langle N_{g,tot}\rangle) \quad (12)$$

(even with permutations b, g, and r). It can now immediately be verified that, from a combination of three auto- and three cross-correlation amplitudes measured in the channels b, g, and r, the seven unknown parameters, N_i ($i = b$, g, r, bg, gr, rb, and bgr), are underdefined. Thus, an additional observable has to be introduced, i.e., the triple-correlation function of

$$G_{bgr}(\tau,\tau') = \langle \delta F_b(t)\delta F_g(t+\tau)\delta F_r(t+\tau')\rangle / (\langle F_b(t)\rangle\langle F_g(t)\rangle\langle F_r(t)\rangle), \quad (13)$$

with the amplitude

$$G_{bgr}(0,0) = \langle \delta N_{bgr}^3(t)\rangle / (\langle N_{b,tot}\rangle\langle N_{g,tot}\rangle\langle N_{r,tot}\rangle). \quad (14)$$

The third central moment of the Poissonian distributed $N_{bgr}(t)$, like the second and all higher moments, just equals the mean, which leaves us with a very simple expression for G_{bgr}, as

$$G_{bgr}(0,0) = \langle N_{bgr}\rangle / (\langle N_{b,tot}\rangle\langle N_{g,tot}\rangle\langle N_{r,tot}\rangle). \quad (15)$$

Interestingly, the number of ternary complexes, N_{bgr}, in the measurement volume V_{eff}, and thus, the local concentration $C_{bgr} = N_{bgr}/V_{eff}$, can now be simply derived from the triple-correlation and the auto-correlation amplitudes as

$$\langle N_{bgr}\rangle = G_{bgr}(0,0)/(G_b(0)G_g(0)G_r(0)). \quad (16)$$

Coincidence analysis for simplified experimental schemes

In cases where only concentrations are to be determined, the time dependences of the above derived auto- and cross-correlation curves are not relevant. This is particularly true for the two-dimensional triple-correlation function $G_{bgr}(\tau,\tau')$, which in contrast to dual auto- and cross-correlation functions cannot be provided by the standard hardware correlators employed in our experiments. Auto-, cross-, and triple-correlation amplitudes ($\tau,\tau' = 0$) are in principle sufficient to determine fractional concentrations of the different species N_i. Thus, the calculation of full temporal correlation functions with varying lag time parameters τ,τ' is not required, and coincidence factors may instead be employed as their recording is significantly simpler, by standard multichannel scalers (Heinze et al., 2002). The so-called double coincidence value, K_2, which has the simple relationship with the cross-correlation amplitude, $K_{ij} = G_{ij}(0) + 1$, is a scalar and represents the relative frequency of coincident events in the two different detection channels. In contrast to the correlation functions discussed above, the calculation of K_2 does not involve the fluctuations but the full recorded fluorescence signals $F_{i,j}(t)$. The same can now accordingly be performed if three rather than two measurement channels are to be investigated. The triple coincidence, K_3, is given by

$$K_3 = \frac{\sum_{ch} F_b(t)F_g(t)F_r(t)}{\sum_{ch} F_b(t)\sum_{ch} F_g(t)\sum_{ch} F_r(t)} \times n_{ch}^2, \quad (17)$$

where the summation is carried out over n_{ch} time channels with binning time τ_{bin} of the fluorescence count-rate trace (Heinze et al., 2002). $n_{ch} \times \tau_{bin}$ is the total measurement time, T_m. For sufficiently small τ_{bin}, the close relationship between fluctuation correlation amplitudes and coincidence factors can immediately be verified:

$$K_3 = \frac{\langle (F_b + \delta F_b(t))(F_g + \delta F_g(t))(F_r + \delta F_r(t))\rangle}{\langle F_b\rangle\langle F_g\rangle\langle F_r\rangle}, \quad (18)$$

$$K_3 = 1 + \frac{\langle \delta F_b\delta F_g\rangle}{\langle F_b\rangle\langle F_g\rangle} + \frac{\langle \delta F_g\delta F_r\rangle}{\langle F_g\rangle\langle F_r\rangle} + \frac{\langle \delta F_r\delta F_b\rangle}{\langle F_r\rangle\langle F_b\rangle} + \frac{\langle \delta F_b\delta F_g\delta F_r\rangle}{\langle F_b\rangle\langle F_g\rangle\langle F_r\rangle}, \quad (19)$$

$$K_3 = 1 + G_{ij}(0) + G_{jk}(0) + G_{ki}(0) + G_{ijk}(0,0). \quad (20)$$

This means that, in the absence of a two-dimensional triple-correlator unit as in our case, all three cross-correlation amplitudes, $G_{ij}(0)$, or double coincidence factors, $K_{ij} = G_{ij}(0) + 1$, and the triple coincidence factor, K_3, are required to determine $G_{ijk}(0,0)$. From determination of $G_{ijk}(0,0)$ and autocorrelation amplitudes, absolute occupation numbers, N_{ijk}, and concentrations, C_{ijk}, can finally be obtained.

A series of coincidence measurements can be described by a Gaussian distribution $D(K)$ given by

$$D(K) = D_{\langle K\rangle}\exp\left(-(K - \langle K\rangle)^2 \Big/ 2\sigma_K^2\right). \quad (21)$$

For many biological applications of multicolor confocal techniques, the primary purpose is to unequivocally distinguish between negative and positive samples before pursuing the challenging task to determine absolute numbers. In the context of coincidence analysis of two- or multimolecular reactions, the separability of the corresponding Gaussian distributions for the start- and the endpoints can be used to assess the resolution of the method. Obviously, the standard deviation of K, σ_K, reflecting the overall signal-to-noise levels, determines the possibility of separating different samples with respect to their concentration of double- or triple-labeled molecules (Heinze et al., 2002).

Simultaneous two-photon excitation of different dyes

Two-photon excitation is induced by quasisimultaneous ($\sim 10^{-15}$ s) arrival of two individual photons within the cross-section of the dye molecule (Denk et al., 1990; Xu and Webb, 1996). Due to the square dependence of the two-photon absorption processes on illumination intensity, the effective excitation volumes are usually much smaller than in the standard one-photon case, minimizing phototoxic effects in irradiated cells and tissue. This inherent spatial sectioning also minimizes probe depletion within the sample, considerably improving measurements in small compartments (Williams et al., 1994; Schwille et al., 1999; Köhler et al., 2000). In addition, advantage can be taken of the experimental finding that two-photon excitation spectra are generally much broader than the corresponding one-photon spectra, allowing for a comfortable performance of multicolor experiments. Recently, we demonstrated that it is in fact possible to excite two spectrally largely distinct dyes with a single IR laser line, and still gain sufficient signal to do reliable single molecule analysis (Heinze et al., 2000).

The photon count rate η in Eq. 3, usually determined in kHz/molecule, is closely related to signal-to-noise ratios in the respective measurements (Koppel, 1974). It is therefore of crucial relevance to optimize this parameter in all detection channels. For simultaneous two-photon excitation of two or more dyes, optimization of all η is performed by varying both the excitation power and wavelength, and looking out for a good compromise in emission efficiencies (Heinze et al., 2000), with maximal brightness and minimal photobleaching of all selected dyes. In addition to that, fast scanning of the excitation beam, i.e., quickly moving the measurement volume element through the sample, has also been shown to dramatically improve the measurement statistics (Winkler et al., 1999).

Experimental setup

The confocal setup (Fig. 1) is based on an inverted Olympus IX-50 microscope combined with a water immersion UplanApo/IR 60 × 1.2 objective (Olympus, Hamburg, Germany) and a self-built detection unit for simultaneous three-color detection. For two-photon excitation, a mode-locked Spectra Physics (Mountain View, CA) Tsunami Ti:Sapphire laser (80 MHz with 100-fs pulses, tunable between 700 and 1000 nm) is employed. The parallel laser light epi-illuminates the objective via a dichroic mirror 725DCSPXR (AHF Analysentechnik, Tübingen, Germany) creating a diffraction-limited focal spot. The size of the resulting detection volume element, V_{eff}, is known from calibration measurements with pure dye TMR (Molecular Probes Europe, Leiden, The Netherlands), excited at 870 nm. Its determination yields a value of 0.3 ± 0.1 fl. Comparable sizes of the three effective volume elements in all three detection channels are verified by additional calibration measurements with the chosen dye system, pure dye solutions Atto 425 (AT425; AttoTec, Siegen, Germany), AlexaFluor 546, and AlexaFluor 633 (A546, A633; Molecular Probes Europe), as explained in the Results section.

The fluorescence light exits the camera port of the microscope and is split by a cascade of dichroic mirrors 530DCLP and 620DCLP (AHF) for triple-color separation. Additional detection light specificity is obtained by bandpass filters (AHF) 485DF70M (channel 1), 580/60M (channel 2), and D680/100 (channel 3), chosen accordingly to the selected dye system. Confocal spectra are recorded with a fiber-coupled spectrometer (Ocean Optics, Duiven, The Netherlands) using an entrance fiber slit of 100 μm. For fluorescence fluctuation analysis, detection is performed by three fiber (diameter: 105 μm) coupled avalanche photodiodes SPCM-AQR-13 (PerkinElmer Instruments GmbH, Rodgau-Jügesheim, Germany). All photon-count signals are electronically split and amplified by a self-built rooter, to simultaneously carry out correlation and coincidence analysis. For simultaneous processing of three auto- and three cross-correlation functions, a custom-made three-channel, multiple-τ correlator unit (Correlator.com, Bridgewater, NJ) is employed. This unit cannot, however, deliver the full temporal triple-correlation function $G_{\mathrm{bgr}}(\tau,\tau')$. Thus, in parallel, all signals

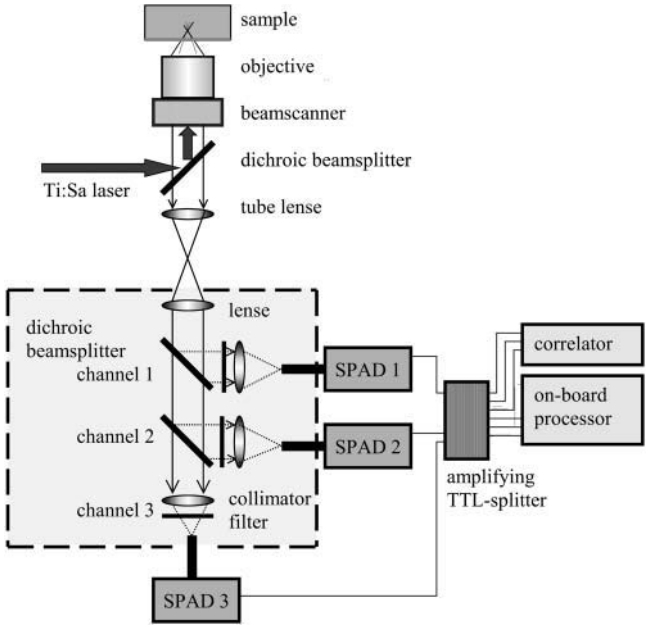

FIGURE 1 Optical setup. Coupled into a high NA objective via a beam-scanning device, a single parallel titanium:sapphire laser line induces the simultaneous excitation of the three differently emitting dye species in buffer solution. The fluorescence is discriminated from laser stray light by a first dichroic mirror and then again spectrally separated in three channels within the detection unit by a cascade of additional dichroic mirrors and emission filters. Detection is provided by three fiber-coupled avalanche photodiodes, the photon count signals evaluated by two alternative processing units. Alternatively, the detectors can be easily replaced by a fiber-coupled spectrometer.

are processed by an on-board multichannel scaler PC card (Adwin 9LD, Jäger Meßtechnik, Lorsch, Germany) for coincidence analysis (Heinze et al., 2002).

Since coincidence analysis is not coupled to the analysis of molecular mobility, the data processing rate and thus, statistical averaging can be improved by inducing fast movements of either the sample or the confocal volume element. A beam scanner device operating at frequencies up to 100 Hz originally developed by Evotec OAI (Hamburg, Germany; Pat. No. WO9748001) was therefore applied in some of the experiments. The quantitative effect of such a beam-scanning device on data quality was previously discussed in detail for a comparable two- photon dual-color application (Heinze et al., 2002).

Biochemical test assay

Upper strand oligonucleotide (201nt, 5′ AAC GCC AGG GTT TTC CCA GTC ACG ACG TTG AAT ATT GAC GGC CAG TGC CAA GCT TGC ATG CCT GCA GGT CGA CTC TAG AGG ATC CCC GGG TAC CGA GCT CGA ATT CGT AAT CAT GGT CAT AGC TGT TTC CTG TGT GAA ATT GTT ATC CGC TCA CAA TTC CAC ACA GCG CTC GAG CCG GAA GCA TAA AGT GTA AAG CCT GGA 3′) was synthesized on an Expedite nucleic acid synthesizer and PAGE purified. Lower strand oligonucleotides (each 66nt, low1: 5′ TGC AGG CAT GCA AGC TTG GCA CTG GCC GTC AAT ATT CAA CGT CGT GAC TGG GAA AAC CCT GGC GTT 3′, low2: 5′ACA GGA AAC AGC TAT GAC CAT GAT TAC GAA TTC GAG CTC GGT ACC CGG GGA TCC TCT AGA GTC GAC 3′, low3: 5′CCA GGC TTT ACA CTT TAT GCT TCC GGC TCG AGC GCT GTG TGG AAT TGT GAG CGG ATA ACA ATT TCA 3′) were custom-synthesized both unmodified and 5′-end-labeled with the

fluorophores AT425 (low1), A546 (low2), and A633 (low3) by IBA (Göttingen, Germany) and double HPLC-purified. All samples contained ~10% of free dye which could not be removed by further purification. Strands were annealed at 10 μM in 50 mM Tris-HCl (pH 7.5) and 150 mM NaCl to yield dsDNA substrates with different combinations of fluorophores. For measurements, samples were diluted in 150 mM KOAc, 37.5 mM Tris-Acetate (pH 7.6), 15 mM MgOAc, 0.75 mM β-mercaptoethanol, 15 μg/ml BSA, and 0.05% (v/v) Triton X-100.

RESULTS

Dye characterization

Besides minimal spectral overlap of the emission spectra, a potential dye combination for triple-color experiments needs to fulfill several photophysical selection criteria (Heinze et al., 2000, 2002) to support simultaneous excitation with a single laser line. Since single line excitation is very restrictive in terms of intensity and wavelength regulation, the most crucial conditions are comparable absorption cross-sections, quantum yields, and photostabilities at the chosen excitation wavelength. Although a good compromise with respect to a common *wavelength* can often be found quite easily because of broad or multiband two-photon excitation spectra, the choice of a common *intensity* is more difficult, especially in the light of future applications in live cells. At any certain excitation wavelength that has been identified as a good compromise, red-emitting dyes are usually much less photostable than their blue or green partners, mainly due to the fact that the energy barriers to higher excited states s_2 or s_3, from which photobleaching is strongly supported, can be more easily overcome by the comparable blue-shifted excitation wavelength.

The dye combination selected for our three-color experiments consists of AT425, A546, and A633. All dyes show sufficient emission yields for a common excitation wavelength of 870 nm without considerable photobleaching. In Fig. 2 *A*, the respective two-photon excited emission spectra ($\lambda_{exc} = 870$ nm) are shown, measured within the focal spot (for each dye independently). As expected, these spectra do not differ significantly from their one-photon-excited counterparts. Considering the shape of the spectra and the distances of their maxima, it becomes apparent that common two-photon excitation is highly preferable with respect to spectral distinction in the visible range: for standard excitation of the two shorter wavelength dyes at their one-photon absorption maxima (425 and 546 nm), the Raman scattering background for these lines would significantly interfere with the respective flanking dye in the red.

To determine the optimal common excitation wavelength, the laser is tuned in 10-nm steps between 720 nm and 970 nm, and the fluorescence efficiency η is determined in kHz/molecule, the pulse width held constant, and the laser intensity adjusted to the respective saturation level for maximal efficiency. This procedure guarantees the identification of ideal excitation conditions both for wavelength and intensity (Heinze et al., 2000). Fig. 2 *B* shows a plot of η versus two-photon excitation wavelength for each dye, measured independently in purified water. The wavelength range for proper triple-color excitation is highlighted.

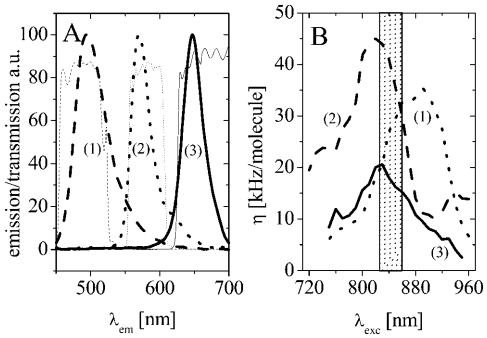

FIGURE 2 (*A*) Emission spectra of the dye system consisting of AT425 (1), A546 (2), and A633 (3) after two-photon excitation at 870 nm. No differences compared to one-photon excitation at the respective absorption maxima can be observed. (*B*) Wavelength dependence of the fluorescence emission yield η in counts per molecule and second for the three dyes under optimal conditions, measured independently in a standard two-photon FCS setup. The pulse width of the laser is kept constant at 100 fs. The excitation power is adapted to the respective fluorescence saturation limit of the dye. The hatched area marks the potential spectral range for common single laser line excitation of all three dyes.

In the combined setup for triple-color measurements, the emission yields for the blue and the green dye in particular are substantially reduced, due to the introduction of proper dichroic mirrors and filters for sufficient spectral separation, but also by the comparably low excitation intensity of only 2.4 mW/cm^2 to avoid photobleaching of the red-emitting A633 (for comparison: the saturation limits for AT425 and A546 are only reached at excitation intensities >4–5 mW/cm^2, data not shown). Accordingly, the optimal wavelength for the following triple-color experiments is determined to be ~870 nm. Under these excitation conditions, the spectral cross-talk between the detection channels amounts to <10% for blue/green and green/red. Hardly any cross-talk (<1%) between blue and red is observed. Table 1 lists the most

TABLE 1 Molecular brightness values, η_i, and cross-talk efficiencies, $c_{ij} = \eta_{rel} = \eta_{j\to i}/\eta_i$ (see Appendix), for the measurement conditions under which the triple-color analysis was performed

Detector	η @ 3.8 mW/cm^2 kHz/molecule	η @ 2.4 mW/cm^2 kHz/molecule	η_{rel} @ 2.4 mW/cm^2 [%]	Background B_i [kHz]
Blue	4 ± 1	1.7 ± 0.5	n.d.	0.3 ± 0.05
Green	5 ± 1.5	2.3 ± 0.5	7 ± 2	0.3 ± 0.05
Red	10 ± 2	8.5 ± 1.5	5 ± 1	0.2 ± 0.05

Note that η_i scale differently with excitation intensities in the chosen regime, as the relative fidelities of the dyes crucially depend on their photophysical properties. At higher intensity, the red dye already starts to saturate and photobleach, where the molecular brightness of the green and blue dye can still be much improved. The conditions in the actual measurements were chosen such that the relative cross-talk could be held well below 10%. Background does not significantly contribute to the measurements.

important parameters for the triple-dye system under two different excitation conditions. At 2.4 mW/cm^2, the count rates per molecule η_i are rather small for the blue and the green dye compared to the red, to minimize spectral cross-talk. If the intensity is, however, raised to 3.8 mW/cm^2, the blue and green dyes increase their relative performance and the contribution of cross-talk can get significant with >10%. To interpret the following experiments, the cross-talk as well as the background are neglected, which can be justified according to Table 1. In cases where these conditions cannot be achieved, the quantitative interpretation of correlation and coincidence amplitudes is much more complicated, as will briefly be outlined in the Appendix.

Checks for proper alignment, dynamic range of the assay

In a multicolor confocal setup, optimal alignment is essential to guarantee maximal overlap of all detection volume elements in the different spectral ranges. This can best be checked by comparison of each two auto- and respective cross-correlation curves for a single dye species, measured simultaneously in two different emission ranges. For perfect overlap, these curves have to be identical (Schwille et al., 1997). In these particular measurements, the excitation intensity was set to 3.8 mW/cm^2 because cross-talk was desirable in this experiment. The data recording time was 60 s. Fig. 3 shows the results for the detection channels ch1/ch2 (Fig. 3 *A*) and ch2/ch3 (Fig. 3 *B*), recorded from AT425 (Fig. 3 *A*) and A546 (Fig. 3 *B*), respectively. As expected, all curves in Fig. 3 *A* and all curves in Fig. 3 *B* are almost perfectly superimposed, proving the identity of the detection volume elements for both channel combinations. In first approximation, considerable overlap for all three channels within the experimental error can thus be assumed, and no systematic reduction of the cross-correlation amplitudes and coincidence values may be expected for the following experiments.

To characterize the dynamic range of the dye combination in terms of separability and spectral cross-talk, cross-correlation and coincidence analysis are performed with a biochemical assay consisting of three labeled oligonucleotides in equal shares; with and without their unlabeled complementary strand for positive and negative controls, respectively. In the positive sample, all probes should be united in a triple complex by quantitatively annealing to the common target. In the negative sample, no triple or even dual complexes can be formed. Both samples are diluted in a TBS-buffer to 69 nM and each measured separately in 10-μl volume in a cover-glass chamber at room temperature. Again, the data recording time was 60 s, but due to the lower mobility of the oligonucleotides compared to the pure dyes, the intensity was now set to 2.4 mW/cm^2 to avoid photobleaching. Fig. 3, *C* and *D*, show typical results of auto- and cross-correlation analysis. The three autocorrelation curves corresponding to the different detection channels

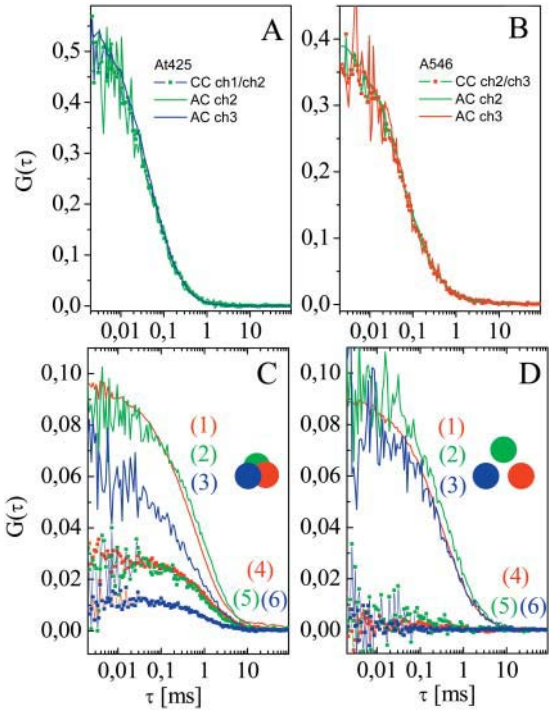

FIGURE 3 Calibration measurements. (*A*, *B*) Controlling the overlap of the excitation and the three detection volume elements, corresponding to the three distinctly emitting fluorophores by auto- and cross-correlation analysis of freely diffusing dye molecules. The perfect overlap of both auto- and cross-correlation curves recorded from different excitation regimes of a single dye guarantees the identity of detection volumes. (*A*) ch1 and ch2 for dye AT425, and (*B*) ch2 and ch3 for dye A546 in the triple-color setup. The identity of detection volumes in ch1 and ch2, as well as ch2 with ch3, allows in first approximation to also assume identity of ch1 with ch3. (*C*, *D*) Auto-correlation and cross-correlation curves recorded from a solution of ternary complexes (*C*) or a mixture of three differently emitting single-labeled DNA oligonucleotides (*D*), resembling the start- and endpoints of the hybridization reaction. The difference in cross-correlation amplitudes in *C* and *D* marks the dynamic performance of the system. Curve legend: (*1*) auto red, (*2*) green, (*3*) blue, (*4*) cross red/green, (*5*) green/blue, and (*6*) blue/red.

(*b*, *g*, and *r*), and the respective cross-correlation curves for all combinations (*b*/*g*, *g*/*r*, and *r*/*b*) were simultaneously detected and calculated in real time with 100-s data recording. From the amplitudes of the auto- and cross-correlation curves, and by knowing the effective measurement volume V_{eff}, absolute concentrations of the dual complexes can be determined by $C_i = N_i/V_{eff}$ (Eq. 10). However, for the proof of principle as intended here, a discussion of relative fractions shall be sufficient. To determine the fraction of species *i* bound to species *j* in the described assay and in the absence of cross-talk, the measured cross-correlation amplitude $G_{ij}(0)$ has to be divided by the autocorrelation amplitude G_j. Also, one has to keep in mind that double-and triple-labeled molecules contribute to $G_{ij}(0)$. The relative numbers of bound molecules are thus given by

$$\frac{(N_{ij} + N_{ijk})}{N_{i,tot}} = G_{ij}(0)/G_j(0).$$

According to this relationship, and with the correlation amplitudes as in Fig. 3 *C*, we find that 33% of all blue molecules have bound to green ones, 32% of all green ones have bound to red ones, and 25% of all red ones have bound blue partners. This is quite a large discrepancy compared to the 100% to be expected for all combinations under optimal assay conditions. One reason for the deviation is the 10% free dye present in all oligomer samples. Another potential reason is the formation of secondary structure motifs in this special DNA target after the binding of one or two oligomers which could inhibit the annealing of a second or third one. However, inasmuch as the calibration measurements reported above basically rule out the possibility of optical artifacts that would lead to similar effects (see Appendix), the reason can only be a biochemical one. The negative control shows basically no cross-correlation signal, as expected for an ideal nonbinding system and perfect spectral separation of emission ranges. Hence, no significant dye cross-talk or unspecific binding of the oligonucleotides can be found to interfere with the specific signals. Herewith, proof of principle for three-color detection under proper optical conditions is demonstrated. However, the cross-correlation measurements could only strictly probe the presence of all respective double pairings, and no evidence for *ternary* complex formation has yet been given. In the following, signal processing is thus turned to dual- and triple-color coincidence analysis, complementing dual-color, cross-correlation measurements as outlined in the Methods section.

Probing ternary complex formation with maximum dynamic range

Utilizing the biochemical assay as described above, identity of dual-color coincidence and cross-correlation measurements can be easily verified. However, to further improve the dynamic range of the measurements, beam-scanning is additionally employed which allows us to increase the fluctuation rate without any change in local concentrations. The influence of beam-scanning is discussed in detail by Heinze et al. (2002). A series of coincidence measurements (100×1 s each) of the positive and negative samples is performed for quantitative assessment of all combinations of oligonucleotides (*b*/*g*, *g*/*r*, *r*/*b*, and *b*/*g*/*r*), summarized in histogram plots (Fig. 4). All measurements were recorded with 40-μs binning time (τ_b) and a beam-scanner frequency of 20 Hz. These conditions have proven to yield optimal results in calibration measurements (not shown). The resulting distributions of the *K*-values were fitted by Gaussian functions (Eq. 21). For the dual coincidences (Fig. 4, *A–C*), excellent separation can be found between the bound samples and the unbound negative controls, without any overlap of two corresponding Gaussian distributions, indicating that neither false-positive nor false-negative events could be detected for total analysis times of 1 s. Obviously, the method shows strong potential for even shorter analysis times, providing a basis for time-resolved studies of fast biochemical reactions as experimentally indicated below.

However, the key feature of true triple-color coincidence analysis is a clear distinction of dual and ternary complexes. The crucial negative control that has thus to be designed consists of a mixture of all dual-color combinations but no triple-color complexes (Fig. 4 *D*). A triple-color mixture consisting of equal amounts of only pairwise-labeled DNA particles serves as the negative control (graphic scheme in Fig. 4 *D*). Here, the absolute concentrations of dual-labeled oligonucleotides are adjusted according to the dye concentrations in the positive sample, to make the discrimination of triple-labeled complexes most evident. To also provide a biochemically similar system, the dual-labeled particles lacking their third binding partner in the negative control are each annealed with an unlabeled complimentary strand.

For positive and negative samples, K_{triple} is now determined following the algorithm outlined above (for measurement parameters, see Fig. 4, *A–C*). Although the overlap is more substantial than in the respective dual-color measurements, the K_{triple} distributions of the positive and negative samples can be clearly separated, which finally proves the principle of the introduced technique, i.e., the possibility to truly distinguish between dual and ternary complexes. The rather large overlap is partly due to the already mentioned nonidealities in assay design, mainly because of incomplete labeling. In an ideal assay system with 100% binding efficiency, the separation quality of the distributions could be improved by more than one order of magnitude. Indications for limited triple-color complex formation were already provided by the calibration measurements with the observed shortcomings in dual complex formation.

Observing and quantifying complexation reactions

So far, a general proof of principle for triple-color cross-correlation and coincidence analysis has been given by opposing positive and negative controls (dual/no dual; ternary/no ternary mixtures). This scheme can now be extended by actually following the *formation* of triple color complexes in real time. This could be achieved by directly monitoring the hybridization kinetics of the three labeled oligonucleotides to a common complementary ssDNA-strand. Hence, a respective association reaction kit providing all fragments in equal amounts of 69 nM in TBS-buffer was analyzed by coincidence analysis at room temperature directly after sample mixing. The reaction conditions were slightly suboptimal at room temperature, but proved sufficient to record considerable association yields. Fig. 5 *A* shows the observed increase of the dual and triple coincidence values during the hybridization process, being clearly distinguishable from the negative controls in Fig. 5 *B*. The negative controls again contained all three different types

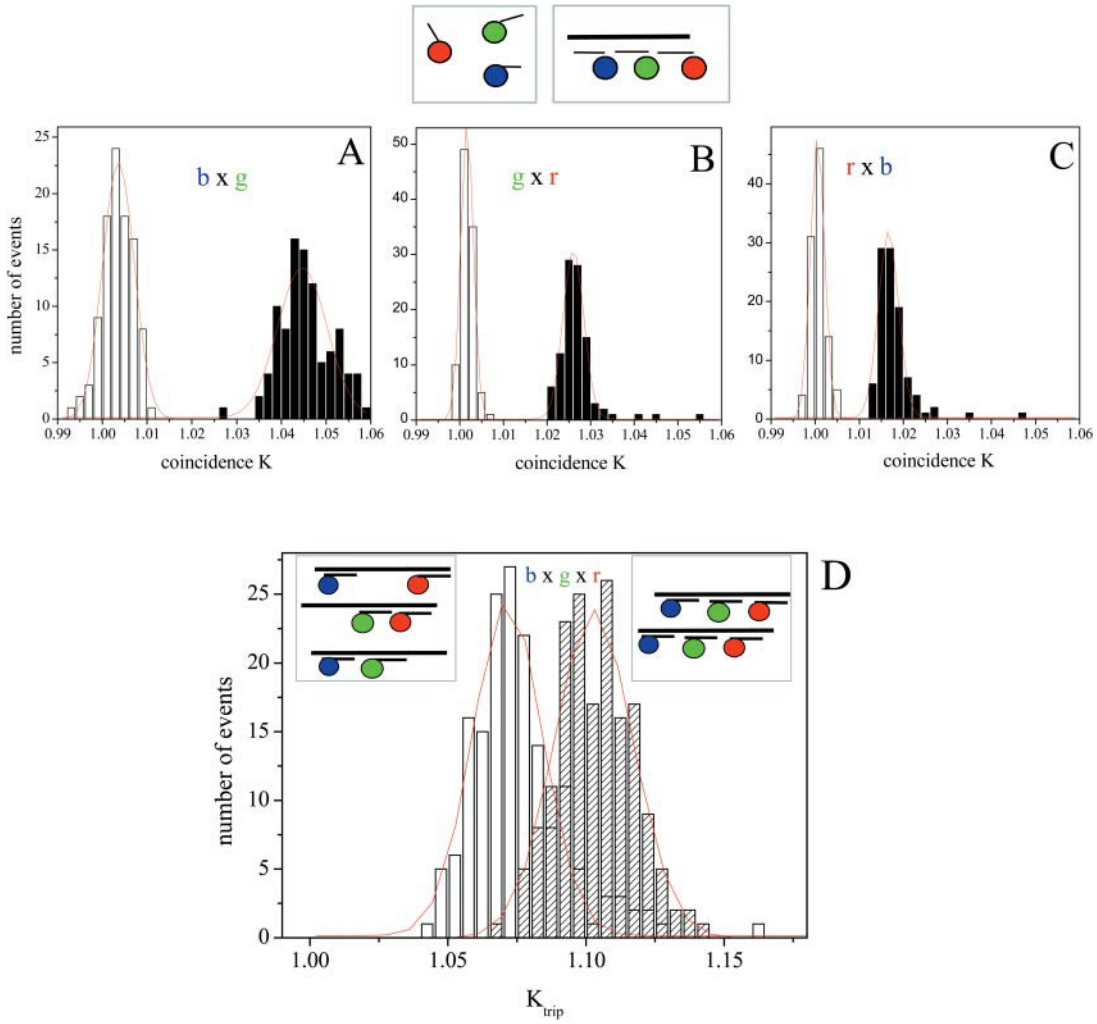

FIGURE 4 (*A–C*): Histogram plots of 100 measurements (1 s each, $\tau_b = 40\ \mu s$) of coincidence values K_2 and K_3 at 20-Hz beam scanner frequency in samples of ternary oligonucleotide probing of a common target (positive sample, *black bars*), and the corresponding mixture of three different, but single-labeled oligonucleotides (negative control, *white bars*). Plots *A–C* refer to the different pairwise coincidences for the triple-color complex sample and the negative control. The histograms were fitted by Gaussian distributions according to Eq. 19, indicating that the technique is well able to distinguish between single- and dual-labeled species in a three-dye system. (*D*) Additional proof of specificity to distinguish between triple- and dual-labeled species in a three-dye system (negative control, *white bars*) and respective ternary complexes (*hatched bars*). Despite the overlap of the distributions, they can be separated sufficiently to distinguish the dual and the ternary cases.

of labeled oligonucleotides with a noncomplementary strand (Fig. 5 *B*) or without any complementary strand (data not shown, qualitatively same result) to check the specificity of the binding. The coincidence values in both controls remain constant on a baseline as expected for ideal nonbinding systems. The difference in baselines accounts for the different background contributions to each of the four coincidence measurements. It also has to be kept in mind that according to Eq. 20, the triple coincidence value, K_3, contains a sum of all dual coincidences, which results in a correspondingly increased baseline for both positive and negative controls.

As its most important feature, coincidence analysis now allows for deriving the absolute particle number and concentration of the ternary complexes at any time directly from the K_3 values in consideration of auto- and cross-correlation amplitudes following Eqs. 18 and 20. Taking all known parameters into account as outlined above, assuming a measurement volume of $V_{eff} = 0.3$ fl as determined by calibration, Fig. 5 *C* summarizes the derived total concentration, C_{ijk}, of ternary complexes during the course of reaction. It can be verified that this absolute concentration is remarkably low, only up to 2 nM in a reaction mix containing 69 nM of labeled sample. However, one again has to keep in mind that the yields of dual complexes already amounted to only ~30% each, due to mentioned non-idealities of the reaction kit. Since the joint probability for ternary complex formation is given by the product of all pairing probabilities, it is not surprising that only such a small amount of triple-labeled product can be observed. The relative low number of triple complexes of only 3% of all

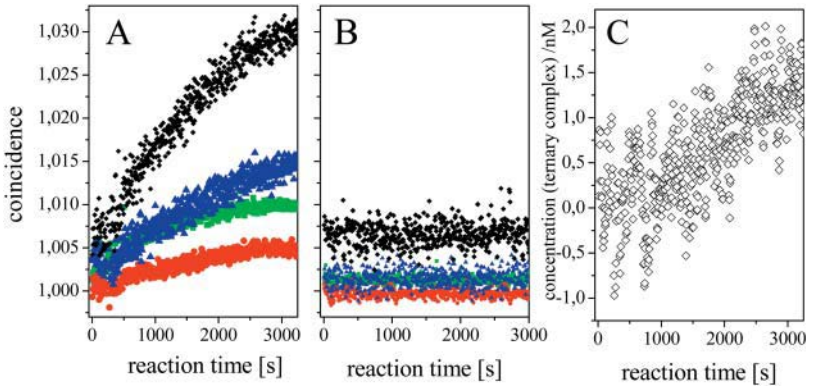

FIGURE 5 Time course of the hybridization reaction of the three oligonucleotides to the complementary ssDNA strand (*A*), and negative control with a noncomplementary strand (*B*) monitored by coincidence analysis for pairwise binding (*blue*, rxg; *green*, gxr; and *red*, rxb) and ternary complex formation (*black*). Total analysis time per coincidence measurement was 6 s ($\tau_b = 40$ μs); beam-scanner frequency was 20 Hz. From coincidence values and simultaneously recorded auto- and cross-correlation amplitudes, the absolute concentration of the triple-labeled complexes can be derived (*C*).

labeled molecules in the reaction mix also accounts for the relatively high variance of C_{ijk} that can be observed in Fig. 5 *C*. However, it already shows the sensitivity of the measurement, where small triple-labeled quantities can be unequivocally probed in presence of a large background of dual- or single-labeled molecules.

Exonuclease

Naturally, neither coincidence analysis nor cross-correlation analysis is limited to simple association reactions that have been studied so far, but both techniques generally work in any case where a physical or chemical linkage is formed or cleaved. To finally confirm the universality of the method, the reaction scheme in the last paragraph should be reversed. Since dissociation processes of nucleic acids can hardly be observed at room temperature, an enzymatic digestion was performed where a readily annealed ternary complex (69 nM) was cleaved by Exonuclease III (215 units/μl). The reaction was monitored by coincidence analysis for few minutes (in the same manner as before for the hybridization reaction. As indicated in Fig. 6 *A*, Exonuclease III destroys the linkage between all involved labeled oligonucleotides, causing a decrease in dual and triple coincidence values. As a negative control, the annealed sample was studied over the same time period as before with no enzyme added. Here, the coincidence values remain constantly high during the whole observation time, confirming that there is no unspecific degeneration of the molecular complex (Fig. 6 *B*).

SUMMARY AND CONCLUSIONS

We successfully show the proof-of-principle of triple-color correlation and coincidence analysis to quantitatively study ternary complex formation. The theoretical framework is presented as well as its successful experimental realization employing two-photon excitation of the three spectrally distinct fluorescent probes with a single IR laser line. As a model system, the hybridization reaction of three differently labeled oligonucleotides to a complementary ssDNA strand, as well as the enzymatic degradation of the complex, could be observed and quantified. It could be shown that ternary complex fractions of well below 5% of labeled molecules are easily identified and quantified. In contrast to other detection methods such as energy transfer approaches, confocal coincidence analysis can be applied to any association or dissociation process or reaction, without any limitations with respect to a certain distance between the fluorophores. Performed in a confocal setup, triple coincidence analysis is a novel and universal optical method for measuring molecular interactions involving more than two species in any transparent environment, and thus also perfectly suited for measurements in live cells.

In the present study, a combination of correlation and coincidence measurements was chosen according to the technical infrastructure. Hardware auto- and cross-correlator units with the potential of online recording, although not strictly required, simplify the alignment of the optical system. However, no triple-correlator recording the full time-dependent $G_{ijk}(\tau,\tau')$ is so far available. If the technique holds its promises for measurements of higher order interactions, the construction of such a module would be highly desirable.

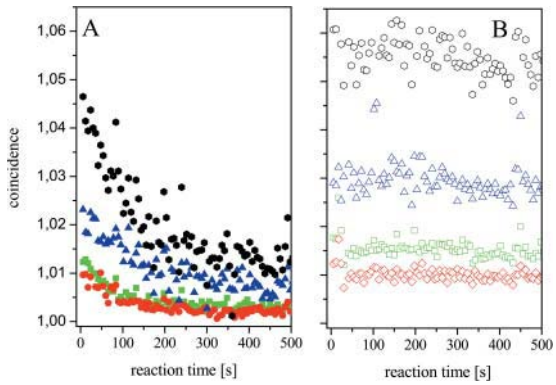

FIGURE 6 Enzymatic cleavage of the readily hybridized triple-color complex. Time course of dual coincidence values (*blue*, rxg; *green*, gxr; and *red*, rxb) and the triple-color coincidence k_3 (*black*) after addition of 0.5 μl Exonuclease III (215 u/μl) (*A*), and negative control without any enzyme treatment (*B*). The coincidence values constantly decrease during the cleavage reaction (*A*) whereas the values for the negative control show constant progression, indicating the presence of stable triple-color complexes without any nonspecific degradation.

A wide variety of fluorescence spectroscopic applications in the biosciences is opened up by exceeding the dual-color schemes and adding a third observable. One interesting potential application is, e.g., provided by an extension of the enzymatic digestion assay explained above. Labeling the enzyme and double-labeling the substrate, Michaelis-Menten complexes, and turnover timescales could be experimentally resolved, and the distinct pathways of enzymatic reactions better understood. Such assays are presently investigated by our group. Further, the simplicity and reliability of the described measurement concept suggests its employment in high-throughput screening where short analysis times per sample and a reduction of parameters are required (Koltermann et al., 1998). In combination with two-photon excitation, FCS and coincidence analysis offer considerable advantages in signal quality, artifact suppression, and reduced cumulative photobleaching, allowing the precise determination of kinetic rates and concentrations of molecular complexes in spatially confined volume elements such as living cells or cell compartments. This provides exciting perspectives for probing receptor complex formation or unraveling intricate processes such as signaling in real time and on a single molecule level.

APPENDIX: DEVIATIONS FROM THE IDEAL CASE

In the Materials and Methods section and the following measurements, several assumptions have been made to allow straight data evaluation. There are many factors that could largely interfere with both the measurement process and the interpretation of the derived results. First, the nonideal overlap of detection volumes would lead to a significant underestimation of the measured double or triple complexes. This was outlined for dual-color analysis before (Schwille, 2001) and is directly transferable to the triple-color case.

Second, in cases where the concentrations cannot be chosen such that the signal always stays well above the background, the amplitudes of auto-, cross-, and triple-correlation curves will be compromised. This has already been outlined by Hom and Verkman for dual-color analysis (Hom and Verkman, 2002). In the presence of background B_i in any detection channel, the fluorescence signals in Eq. 3 have to be changed into

$$F_b(t) = \eta_b(N_b(t) + N_{bg}(t) + N_{rb}(t) + N_{bgr}(t)) + B_b = S_b + B_b$$

$$F_g(t) = \eta_g(N_g(t) + N_{bg}(t) + N_{gr}(t) + N_{bgr}(t)) + B_g = S_g + B_g$$

$$F_r(t) = \eta_r(N_r(t) + N_{gr}(t) + N_{rb}(t) + N_{bgr}(t)) + B_r = S_r + B_r,$$

where the auto- and cross-correlation amplitudes are now given by

$$G_i(0) = \frac{\eta_i S_i}{(S_i + B_i)^2} \quad G_{ij}(0) = \frac{\eta_i \eta_j (N_{ik} + N_{ijk})}{(S_i + B_i)(S_j + B_j)}.$$

The triple-correlation amplitude is then accordingly

$$G_{bgr}(0,0) = \frac{\eta_b \eta_g \eta_r N_{bgr}}{(S_b + B_b)(S_g + B_g)(S_r + B_r)}.$$

The triple-color correlation and coincidence amplitudes are thus reduced by the following factor,

$$\frac{G_{bgr,measured}}{G_{bgr,real}} = \frac{1}{(1 + B_b/S_b)(1 + B_g/S_g)(1 + B_r/S_r)}.$$

To quantify the effect on the extracted numbers N_{bgr}, the G_i and G_{ij} have to be additionally considered. This is a straightforward task that can be left to the reader.

Finally, a large amount of spectral cross-talk, which could in our case also be neglected, introduces substantial complications if relative and total numbers of particles of different species are to be derived. Auto- and cross-correlation as well as triple-correlation amplitudes are affected. If we assume cross-talk from blue to green with a count rate per molecule $\eta_{b\to g}$ and from green to red with a count rate $\eta_{g\to r}$, neglecting cross-talk from blue to red, all other contaminations from long wavelength to short wavelength dyes, and for simplicity the background, the intensities in the three channels have to be changed to

$$F_b(t) = \eta_b(N_b(t) + N_{bg}(t) + N_{rb}(t) + N_{bgr}(t)) = \eta_b N_{b,tot}$$

$$\begin{aligned} F_g(t) &= \eta_g(N_g(t) + N_{bg}(t) + N_{gr}(t) + N_{bgr}(t)) + \eta_{b\to g}(N_b(t) \\ &\quad + N_{bg}(t) + N_{rb}(t) + N_{bgr}(t)) \\ &= \eta_g N_{g,tot} + \eta_{b\to g} N_{b,tot} \end{aligned}$$

$$\begin{aligned} F_r(t) &= \eta_r(N_r(t) + N_{gr}(t) + N_{rb}(t) + N_{bgr}(t)) + \eta_{g\to r}(N_g(t) \\ &\quad + N_{bg}(t) + N_{gr}(t) + N_{bgr}(t)) \\ &= \eta_r N_{r,tot} + \eta_{g\to r} N_{g,tot}. \end{aligned}$$

We then obtain the following expressions for auto-, cross-, and triple-correlation amplitudes in the real (including cross-talk) compared to the ideal cases,

$$G_{b,real}(0) = G_{b,ideal}(0) = \frac{1}{N_{b,tot}}$$

$$G_{g,real}(0) = \frac{N_{g,tot} + A_g}{(N_{g,tot} + B)^2} \text{ against } G_{g,ideal}(0) = \frac{N_{g,tot}}{N_{g,tot}^2}$$

$$G_{r,real}(0) = \frac{N_{r,tot} + A_r}{(N_{r,tot} + C)^2} \text{ against } G_{r,ideal}(0) = \frac{N_{r,tot}}{N_{r,tot}^2}$$

$$G_{bg,real}(0) = \frac{(N_{bg} + N_{bgr}) + B}{N_{b,tot}(N_{g,tot} + B)} \text{ against } G_{bg,ideal}(0) = \frac{(N_{bg} + N_{bgr})}{N_{b,tot} N_{g,tot}}$$

$$G_{gr,real}(0) = \frac{(N_{gr} + N_{bgr}) + C}{N_{g,tot}(N_{r,tot} + C)} \text{ against } G_{gr,ideal}(0) = \frac{(N_{gr} + N_{bgr})}{N_{g,tot} N_{r,tot}}$$

$$G_{br,real}(0) = \frac{(N_{br} + N_{bgr}) + D_{br}}{N_{b,tot}(N_{r,tot} + C)} \text{ against } G_{br,ideal}(0) = \frac{(N_{br} + N_{bgr})}{N_{b,tot} N_{r,tot}}$$

$$G_{bgr,real}(0,0) = \frac{N_{bgr} + E_{bgr}}{N_{b,tot}(N_{g,tot} + B)(N_{r,tot} + C)} \text{ against}$$

$$G_{bgr,ideal}(0) = \frac{N_{bgr}}{N_{b,tot} N_{g,tot} N_{r,tot}}.$$

The correction factors are given by

$$A_g = 2c_{bg}(N_{bg} + N_{bgr}) + c_{bg}^2 N_{b,tot}$$

$$A_r = 2c_{gr}(N_{gr} + N_{bgr}) + c_{bg}^2 N_{g,tot}$$

$$B = c_{bg} N_{b,tot}$$

$$C = c_{gr} N_{g,tot}$$

$$D_{br} = c_{gr}(N_{bg} + N_{bgr})$$

$$E_{bgr} = c_{gr}(N_{bg} + N_{bgr}) + c_{bg}(N_{br} + N_{bgr}) + c_{bg}c_{gr}(N_{bg} + N_{bgr}),$$

with the relative cross talk blue to green, $c_{bg} = \eta_{b\to g}/\eta_g$, and from green to red, $c_{gr} = \eta_{g\to r}/\eta_r$. These values are, in our cases, well below 10% (see Table 1). In evaluating this set of equations, it can be verified that the relationship between the determined and the actual values N_i ($i = g, r, bg, gr$, and bgr) is nonlinear and precise knowledge about $N_{i,tot}$, c_{bg}, and c_{gr} is required. Thus, the suppression of cross-talk, as achieved in our case by increasing the relative fidelity of the red with respect to the green and blue dyes, is highly advisable.

We thank Elke Haustein and Sally Kim for helpful discussions, and Karin Birkenfeld for assistance with sample preparation.

We gratefully acknowledge financial support by the German Ministry for Education and Research (Biofuture grants 0311845 and 16SV1257) and Evotec OAI (Hamburg, Germany).

REFERENCES

Bacia, K., I. V. Majoul, and P. Schwille. 2002. Probing the endocytic pathway in live cells using dual-color fluorescence cross-correlation analysis. *Biophys. J.* 83:1184–1193.

Bieschke, J., A. Giese, W. Schulz-Schaeffer, I. Zerr, S. Poser, M. Eigen, and H. Kretzschmar. 2000. Ultrasensitive detection of pathological prion protein aggregates by dual-color scanning for intensely fluorescent targets. *Proc. Natl. Acad. Sci. USA.* 97:5468–5473.

Clegg, R. M. 1996. Fluorescence resonance energy transfer. *In* Fluorescence Imaging Spectroscopy and Microscopy. X. F. Wang and B. Herman, editors. John Wiley & Sons, New York. 179–252.

Demandolx, D., and J. Davoust. 1997. Multicolor analysis and local image correlation in confocal microscopy. *J. Microsc.* 185:21–36.

Denk, W., J. H. Strickler, and W. W. Webb. 1990. Two-photon laser scanning fluorescence microscopy. *Science.* 248:73–76.

Eigen, M., and R. Rigler. 1994. Sorting single molecules: application to diagnostics and evolutionary biotechnology. *Proc. Natl. Acad. Sci. USA.* 91:5740–5747.

Elson, E. L., and D. Magde. 1974. Fluorescence correlation spectroscopy. I. Conceptual basis and theory. *Biopolymers.* 13:1–27.

Heinze, K. G., A. Koltermann, and P. Schwille. 2000. Simultaneous two-photon excitation of distinct labels for dual-color fluorescence cross-correlation analysis. *Proc. Natl. Acad. Sci. USA.* 97:10377–10382.

Heinze, K. G., M. Rarbach, M. Jahnz, and P. Schwille. 2002. Two-photon fluorescence coincidence analysis: rapid measurements of enzyme kinetics. *Biophys. J.* 83:1671–1681.

Hom, E. F. Y., and A. S. Verkman. 2002. Analysis of coupled bimolecular reaction kinetics and diffusion by two-color fluorescence correlation spectroscopy: enhanced resolution of kinetics by resonance energy transfer. *Biophys. J.* 83:533–546.

Kettling, U., A. Koltermann, P. Schwille, and M. Eigen. 1998. Real-time enzyme kinetics monitored by dual-color fluorescence cross-correlation spectroscopy. *Proc. Natl. Acad. Sci. USA.* 95:1416–1420.

Köhler, R. H., P. Schwille, W. W. Webb, and M. R. Hanson. 2000. Active protein transport through plastid tubules: velocity quantified by fluorescence correlation spectroscopy. *J. Cell Sci.* 113:3921–3930.

Koltermann, A., U. Kettling, J. Bieschke, T. Winkler, and M. Eigen. 1998. Rapid assay processing by integration of dual-color fluorescence cross-correlation spectroscopy: high throughput screening for enzyme activity. *Proc. Natl. Acad. Sci. USA.* 95:1421–1426.

Koppel, D. E. 1974. Statistical accuracy in fluorescence correlation spectroscopy. *Phys. Rev. A.* 10:1938–1945.

Lippincott-Schwartz, J., E. Snapp, and A. Kenworthy. 2001. Studying protein dynamics in living cells. *Nat. Rev. Mol. Cell Biol.* 2:444–456.

Magde, D., E. L. Elson, and W. W. Webb. 1972. Thermodynamic fluctuations in a reacting system—measurement by fluorescence correlation spectroscopy. *Phys. Rev. Lett.* 29:705–708.

Manders, E. M. M., F. J. Verbeek, and J. A. Aten. 1993. Measurement of co-localization of objects in dual-color confocal images. *J. Microsc.* 169:375–382.

Pawley, J. 1995. Handbook of Biological Confocal Microscopy, 2nd Ed. Plenum Press, New York.

Periasamy, A. 1998. Digital deconvolution FRET microscopy: 3D visualization of protein-protein interactions in a single living cell. *SPIE.* 3260:1–9.

Peterson, N. O., D. C. Johnson, and M. J. Schlesinger. 1986. Scanning fluorescence correlation spectroscopy. II. Application to virus glycoprotein aggregation. *Biophys. J.* 49:817–820.

Rigler, R., Z. Foldespapp, F. J. Meyeralme, C. Sammet, M. Volcker, and A. Schnetz. 1998. Fluorescence cross-correlation—a new concept for polymerase chain reaction. *J. Biotechnol.* 63:97–109.

Schwille, P., F.-J. Meyer-Almes, and R. Rigler. 1997. Dual-color fluorescence cross-correlation spectroscopy for multicomponent diffusional analysis in solution. *Biophys. J.* 72:1878–1886.

Schwille, P., U. Haupts, S. Maiti, and W. W. Webb. 1999. Molecular dynamics in living cells observed by fluorescence correlation spectroscopy with one- and two-photon excitation. *Biophys. J.* 77:2251–2265.

Schwille, P. 2001. Cross-correlation analysis in FCS. *In* Fluorescence Correlation Spectroscopy. Theory and Applications. E. L. Elson and R. Rigler, editors. Springer, Berlin, Germany. 360–378.

Selvin, P. R. 2002. Fluorescence resonance energy transfer. *Meth. Enzymol.* 246:300–334.

Williams, R. M., D. Piston, and W. W. Webb. 1994. Two-photon molecular excitation provides intrinsic 3-dimensional resolution for laser-based microscopy and microphotochemistry. *FASEB J.* 8:804–813.

Winkler, T., U. Kettling, A. Koltermann, and M. Eigen. 1999. Confocal fluorescence coincidence analysis: an approach to ultra high-throughput screening. *Proc. Natl. Acad. Sci. USA.* 96:1375–1378.

Wiseman, P. W., J. A. Squier, M. H. Ellisman, and K. R. Wilson. 2000. Two-photon image correlation spectroscopy and image cross-correlation spectroscopy. *J. Microsc.* 200:14–25.

Wouters, F. S., P. J. Verveer, and P. I. H. Bastiaens. 2001. Imaging biochemistry inside cells. *Trends Cell Biol.* 11:203–211.

Xu, C., and W. W. Webb. 1996. Measurement of two-photon excitation cross sections of molecular fluorophores with data from 690 to 1050 nm. *J. Opt. Soc. Am. B.* 13:481–491.